ACS APPLIED MATERIALS & INTERFACES

Research Article

www.acsami.org

Highly Sensitive, Uniform, and Reproducible Surface-Enhanced Raman Spectroscopy Substrate with Nanometer-Scale Quasi-periodic Nanostructures

Yuanhao Jin,[†,‡,#] Yingcheng Wang,[†,‡,#] Mo Chen,[†,‡] Xiaoyang Xiao,[†,‡] Tianfu Zhang,[†,‡] Jiaping Wang,[†,‡] Kaili Jiang,[†,‡] Shoushan Fan,[†,‡] and Qunqing Li*[,†,‡]

[†]State Key Laboratory of Low-Dimensional Quantum Physics, Department of Physics & Tsinghua-Foxconn Nanotechnology Research Center, Tsinghua University, Beijing 100084, China

[‡]Collaborative Innovation Center of Quantum Matter, Beijing 100084, China

Supporting Information

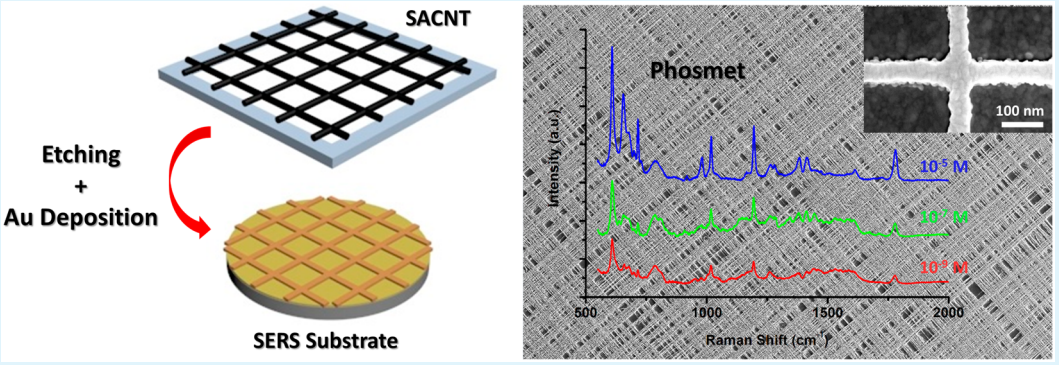

ABSTRACT: We introduce a simple and cost-effective approach for fabrication of effective surface-enhanced Raman spectroscopy (SERS) substrates. It is shown that the as-fabricated substrates show excellent SERS effects in various probe molecules with high sensitivity, that is, picomolar level detection, and also good reliability. With a SERS enhancement factor beyond 10^8 and excellent reproducibility (deviation less than 5%) of signal intensity, the fabrication of the SERS substrate is realized on a four-inch wafer and proven to be effective in pesticide residue detection. The SERS substrate is realized first through the fabrication of quasi-periodic nanostructured silicon with dimension features in tens of nanometers using superaligned carbon nanotubes networks as an etching mask, after which a large amount of hot spots with nanometer gaps are formed through deposition of a gold film. With rigorous nanostructure design, the enhanced performance of electromagnetic field distribution for nanostructures is optimized. With the advantage of cost-effective large-area preparation, it is believed that the as-fabricated SERS substrate could be used in a wide variety of actual applications where detection of trace amounts is necessary.

KEYWORDS: *silicon nanostructure, surface-enhanced Raman spectroscopy, superaligned carbon nanotubes, pesticide residue detection, SERS substrate*

INTRODUCTION

In the 1970s, Raman signals were found to be enhanced on a roughened silver surface by a factor of 10^5–10^6.[1,2] In the application for ultrasensitive identification of analytes, surface-enhanced Raman spectroscopy (SERS) has been continuously developed and widely used as one of the most promising techniques as an analytical tool in analytic identification of trace amounts and even single-molecule level detection.[3,4] As a Raman shift reflects chemical bond vibration in analytes, most chemical species can be identified and studied in theory.[5,6] Thus, SERS is widely used as a versatile analytical tool in the fields of chemical and biochemical analysis.[7−11]

It is widely recognized that relatively huge electromagnetic fields are induced in nanogaps between nanoparticles and sharp tips of noble-metal nanostructures, also called "hot spots" in SERS applications, which generate comparably enhanced Raman signals from analytes.[12,13] It has been reported that metallic nanoparticles dispersed in a colloidal solution have an enhancing effect on Raman signals in which these are located sufficiently close to each other, that is, always on the order of a few nanometers.[14−16] However, compared with currently fabricated metallic nanoparticles in colloidal solutions, hot spots generated by nanostructures on substrates possess more uniform distribution and usually higher density; these are known as SERS substrates.[17−19] These substrates are more convenient for sample preparation and storage in actual

Received: June 19, 2017
Accepted: August 30, 2017
Published: August 30, 2017

DOI: 10.1021/acsami.7b08807
ACS Appl. Mater. Interfaces 2017, 9, 32369−32376

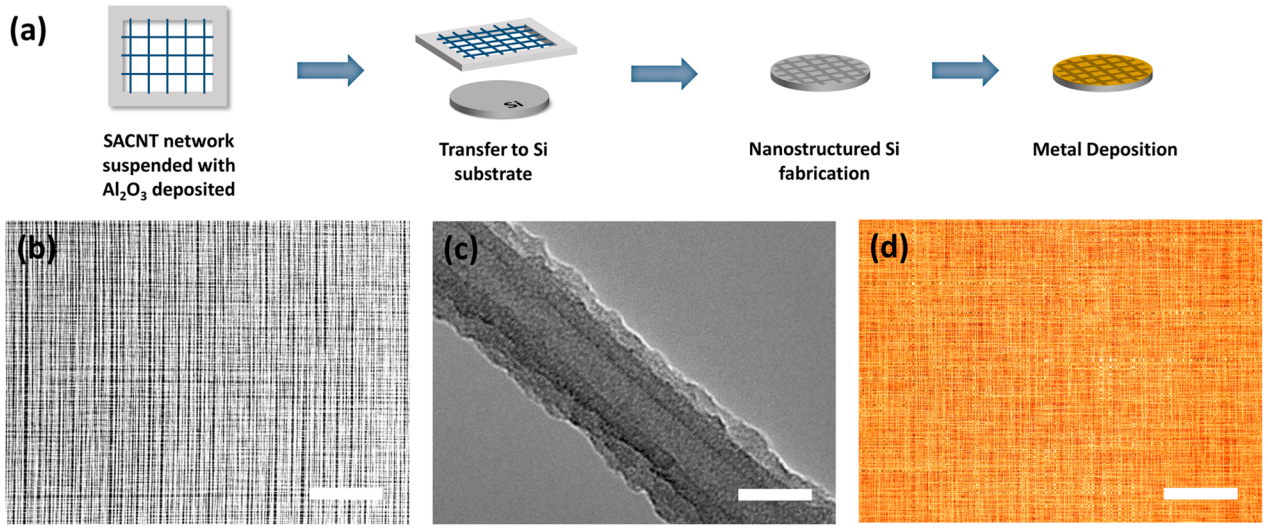

Figure 1. (a) Schematic illustration of the process used to fabricate SERS substrates. (b) SEM image of cross-stacked SACNT films, 100 μm scale bar. (c) TEM image of a CNT from SACNT films coated with 20 nm of Al_2O_3, 20 nm scale bar. (d) Microscope image of SERS substrate in large scale, 1 mm scale bar.

applications;[20] thus, great efforts have been made to fabricate SERS substrates by diverse nanofabrication methods, including electron beam lithography, chemical etching, and mechanical deformation.[21−24] Although these fabrication methods offer hot spots with precision and stability, they suffer from high fabrication costs and moderate throughput.[25−30] Ideally, a SERS substrate should sufficiently enhance the Raman signals while maintaining high uniformity and reproducibility for applications. Thus, during the fabrication of SERS substrates, there is always a trade-off between signal enhancement and product reproducibility. When focusing on uniformity and reproducibility in actual applications, relatively lower enhancement tends to be realized, and vice versa. In addition, because of technical limitations in large-area nanofabrication with high quality, especially at low cost, there are still barriers to SERS applications as consumables in both laboratory and industry settings. On the whole, SERS applications suffer from a lack of reliable SERS substrates. It is therefore essential that nanostructures with excellent electromagnetic characteristics can be fabricated uniformly in large areas in a cost-effective way.

Herein, this study presents a routine sample preparation method for producing highly sensitive, uniform, and reproducible SERS substrates at low cost. More importantly, this fabrication method can be scaled up to wafer level without difficulty. Quasi-periodic nanostructures with dimension features of tens of nanometers are first fabricated on a silicon surface with super aligned carbon nanotube (SACNT) films used as an etching mask, and a metal layer is then deposited on the nanostructures to form nanometer gaps. Simulation results show that the electromagnetic field intensity dramatically increases at the interface of silicon−metal nanostructures and "hot spots" with high yield are supplied because of the unique morphology of the as-fabricated nanostructures. According to the simulation results, the structure parameters of the SERS substrate can be further optimized, and it is shown that a Rhodamine 6G (R6G) molecule can be detected with the lowest concentration of 10^{-13} mol/L (M). In particular, the SERS substrate can be used to detect pesticide residue such as phosmet with a detection limit of as low as 0.001 μM (0.3 ppb), which is much lower than the maximal residue limit for food safety (7 ppm, U.S. Environmental Protection Agency, EPA). The superior performance of the SERS substrate is attributed to the high-density quasi-periodic nanostructures and thus abundant hot spots for SERS applications, which also provides insurance with respect to the reliability and reproducibility of this detection method. Furthermore, as a fabrication method on the wafer scale at low cost, we focus on demonstrating the production of this SERS substrate in a simple, uniform, and cost-effective way using standard silicon processing equipment. This SERS substrate can be useful in detecting trace amounts in actual applications.

EXPERIMENTAL RESULTS

SACNT networks were used as a mask in the silicon etching process for the first time, and the fabrication scheme is shown in Figure 1a. A SACNT film was pulled out from a carbon nanotube (CNT) array with a height of 300 μm grown on an 8 in. silicon wafer.[31] SACNT film fabrication can be performed automatically and continuously, which guarantees that it can be prepared conveniently in large quantities in a cost-effective manner so that related research could be more readily achieved in actual applications (more details shown in Figure S1 of the Supporting Information, including the fabrication process of SACNT films and its morphology).[32,33] The CNTs in SACNT films were aligned and uniformly formed quasi-periodic nanostructures on a large scale. SACNT films were cross-stacked on a metal frame to form SACNT networks. A SEM image of the SACNT networks is depicted in Figure 1b.

SACNT networks can be processed in a suspended manner over large areas, which is one of the advantages of this material system. In a previous study by our group, SACNT networks coated with metal oxide were shown to be effective as an etching mask in the reactive ion etching (RIE) process.[34,35] Herein, according to the silicon nanostructure fabrication conditions, Al_2O_3 with a thickness of 20 nm was deposited on suspended SACNT networks through e-beam deposition. With the advantage that SACNT networks are prepared in a suspended manner, CNTs will be coated completely by the metal oxide to ensure their role as a mask in a later etching process. As shown in the transmission electron microscope (TEM) image in Figure 1c, every single carbon nanotube in the SACNT networks was completely wrapped by Al_2O_3 so that the deposited SACNT networks could be regarded as Al_2O_3 nanowire networks. This ensures that the deposited SACNT networks are effective as an etching mask during the later silicon etching process in a SF_6 atmosphere because of the

DOI: 10.1021/acsami.7b08807
ACS Appl. Mater. Interfaces 2017, 9, 32369−32376

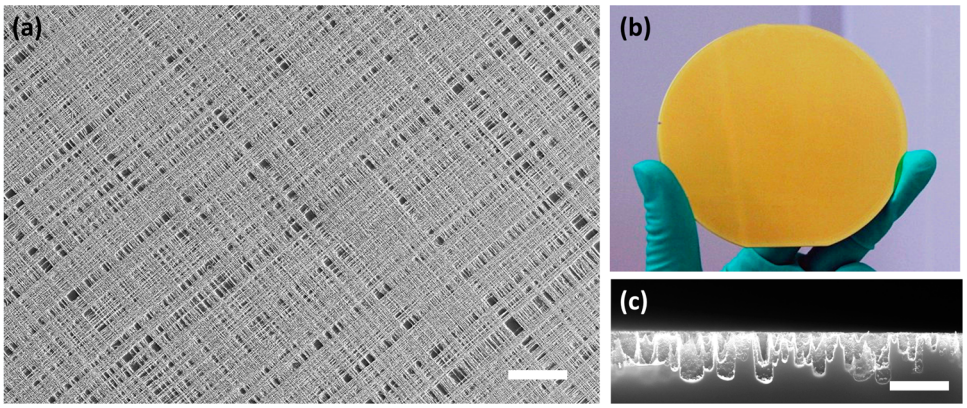

Figure 2. (a) SEM images of SERS substrate with dimension features of SACNT networks with scale bars of 100 μm. (b) SERS substrate fabrication realized on 4 in. silicon wafer. (c) SEM image of the substrate from side angle, 500 nm scale bar.

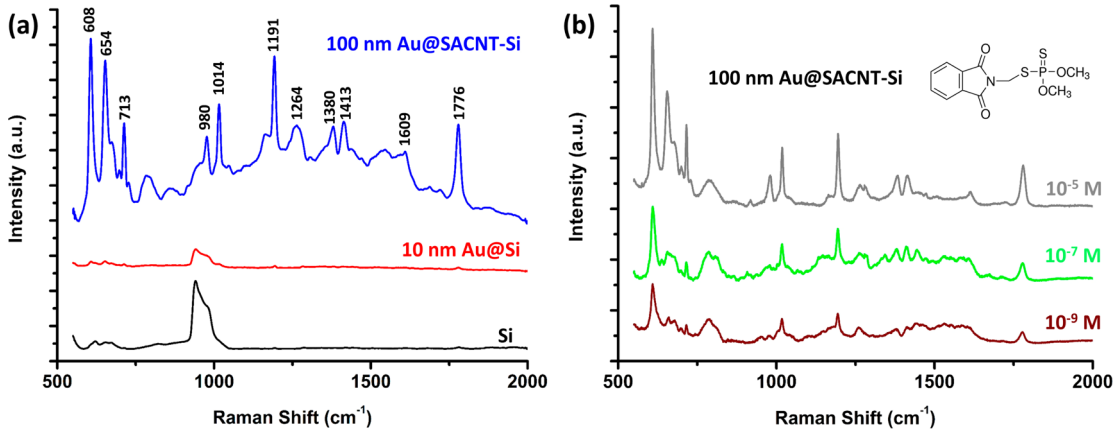

Figure 3. (a) Raman spectra of phosmet with concentration of 10^{-4} M on SERS substrate, Au−silicon substrate, and silicon, respectively. (b) Raman spectra of phosmet on SERS substrate performed with molecule concentrations from 10^{-5} to 10^{-9} M (from top to bottom). Laser wavelength 785 nm, excitation intensity 8 mW, data acquisition time 10 s.

high selectivity for Al_2O_3 materials. This unique advantage will greatly extend the application range of this fabrication method. According to the etching parameters, such as etching gases and conditions, corresponding materials can be chosen to be deposited on suspended SACNT networks or films. This process forms a quasi-periodic etching mask with dimension features of tens of nanometers, which can be prepared over a large area and is suitable for most fabrication situations. It is shown that the morphology of SACNT networks could be realized on intended substrates with this fabrication method, and extensive prospects for further application have the potential to be realized based on various materials with excellent nanostructures.

Then the deposited SACNT networks were transferred to a silicon substrate and alcohol was applied to the interface between the SACNT network and silicon to make the CNTs shrink and bind more strongly with the silicon. The silicon etching process was carried out in an inductively coupled plasma (ICP) etching system with SF_6 gas for etching and C_4F_8 for protection (the detailed parameters and etching process are shown in Figure S2a). SACNT networks were removed in an acetone ultrasonic bath after silicon etching. For contamination removal, substrates were exposed to argon plasma to physically remove remnants and decomposition products. After the etching process, the dimensional features of the SACNT networks were completely transferred to silicon substrates over a large area. After standard processing in piranha solution for further cleaning, a gold (Au) layer was deposited on the as-fabricated silicon substrate through e-beam deposition, as shown in the microscope image in Figure 1d. The metallization thickness was optimized, and further discussion is presented as follows. Here, the silicon nanostructure depth was set to 500 nm and Au layer of 100 nm was deposited on the substrates. The whole fabrication process is relatively simple, including the "etching" and "metal deposition" processes. With use of this approach, Au−silicon nanostructure substrates are realized over a large area with standard silicon etching and metal deposition processes.

In detail, the morphology of the as-fabricated substrate is shown in the SEM image in Figure 2a. Lines on the scale of tens of nanometers were formed on the silicon material in a cross manner; however, there is no junction between lines because of the integrated top-down etching method. High nanostructure uniformity was obtained over a large area. As shown in Figure 2b, the fabrication of the SERS substrates has been uniformly realized in a 4 in. silicon wafer. Additionally, a SEM image of the substrate from a side angle is shown in Figure 2c, which illustrates that the side walls of the nanostructures were also completely covered by the Au layer. The depth of the as-fabricated nanostructures is related to the etching time and can be controlled accurately (as illustrated in Figure S2b).

An attempt was made to explore the use of such an easily fabricated nanostructure in application as a SERS substrate. We chose the analysis of pesticide residue as our target and tried to establish a rapid detection method for low concentrations using Raman spectroscopy. Because of its sensitivity and reliable identification of molecular structures, Raman technology has been widely used in recent years in routine application fields including food safety, explosives detection, and biotechnology.[36−39] Pesticide residue in fruits and vegetables is one of the major food safety concerns in modern agriculture, and if the amount of pesticides is above the set tolerance levels (from 0.1 to 50 ppm, EPA), there could be a threat to human health. However, it is rather difficult to realize chemical detection of various kinds of pesticide residue in a rapid, accurate, and cost-effective manner.[36,37]

DOI: 10.1021/acsami.7b08807
ACS Appl. Mater. Interfaces 2017, 9, 32369−32376

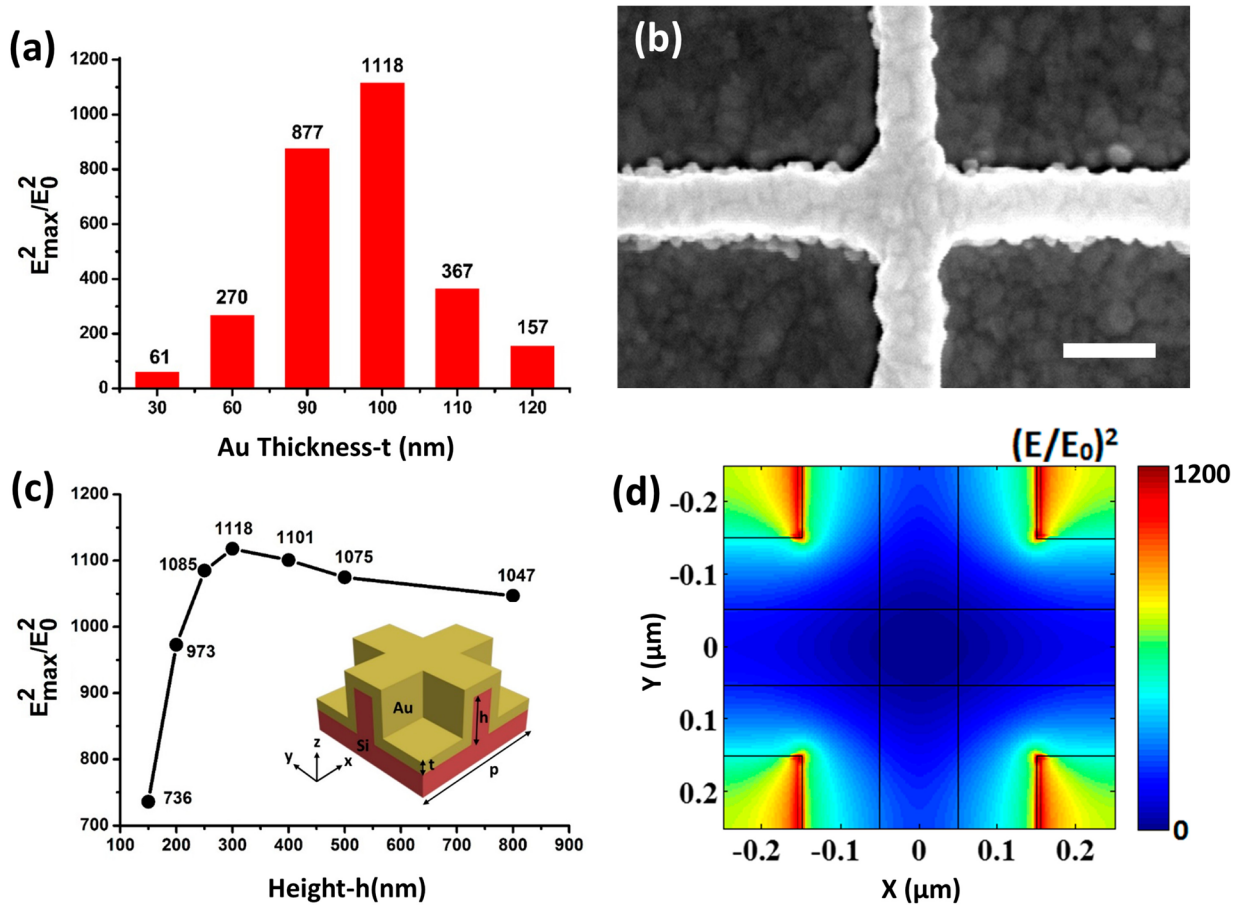

Figure 4. Calculated electromagnetic field distribution and intensity of Au−silicon nanostructures. (a) Histograms of field enhancements calculated for Au−silicon nanostructures with Au thicknesses of 30−120 nm. (b) SEM image of Au−silicon nanostructures in local detail with scale bar of 100 nm. (c) Calculated electromagnetic field enhancements for Au−silicon nanostructures with corresponding depth. Schematic view inset showing the simplified unit model for calculation. (d) Calculated electromagnetic field distribution and intensity of Au−silicon nanostructures with Au thickness of 100 nm and depth of 500 nm, respectively.

Previously, SERS technology has shown great potential for detection of pesticide residue at trace amounts. However, the sensitivity, reproducibility, and reliability of SERS substrates remain inescapable problems in this situation.[38,39]

As one of the main organophosphate pesticides commonly used in agriculture, phosmet has a relatively long residual period at normal temperature and its residuals are harmful to human health. For investigation of the sensitivity detection of the SERS substrate, phosmet was chosen as a probe molecule for SERS measurements, which is regarded as one of the key challenges in pesticide residue detection. A 10^{-4} M aqueous solution of phosmet (Alfa Aesar) in methanol was prepared and a drop of 20 μL was applied to the as-fabricated SERS substrate. Both 10 nm Au-coated bare silicon and a bare silicon substrate were prepared in the same way for comparison. After the complete evaporation of liquid, the Raman spectra were acquired with a 785 nm laser under 8 mW power through a 100× objective lens (NA 0.9), and the laser spot was 10 μm^2. As shown in Figure 3a, peaks associated with the phosmet molecule could be identified clearly on the SERS substrate and were enhanced greatly compared with Raman spectra measured on Au-coated bare silicon and bare silicon surfaces. Furthermore, as the concentration of phosmet molecules in pesticide residues is always extremely low, it is also necessary to investigate the sensitivity performance of the as-fabricated SERS substrates. The phosmet solution was continuously diluted to 10^{-9} M, corresponding to ppb level in mass fraction, and the Raman spectra were acquired as in the previous setup. As shown in Figure 3b, with an extremely low phosmet concentration of 10^{-9} M, the Raman peaks could also be identified clearly. Currently, chromatography methods are used widely in the detection of pesticide residue; however, the detection process is always complicated and requires too much time or cost.[34] Generally, the tolerance set for phosmet residues in fruits is as low as 0.1 mg/g, depending on the species. Herein, it is shown that the detection of phosmet pesticide residue could be realized at ppb level with the as-fabricated SERS substrate, and it is believed that this substrate will have wider prospects in routine application fields.

Because phosmet as a pesticide residue could be detected with the as-fabricated SERS substrate at extremely low concentrations, it would be meaningful to understand why such a network nanostructure can be used as a SERS substrate because it can be fabricated at large scale with very good uniformity and low cost. To analyze the underlying physics of the observed extremely great enhancement down to ppb level, theoretical analysis and calculation of electromagnetic fields were performed on the as-fabricated nanostructures. Although the SEM investigation results showed that the quasi-periodic nanostructure is formed of cross-stacked lines, lacking nanogaps and nanotips at the substrate surface, there are many corners between the nanolines. Therefore, we employed finite difference time domain (FDTD) simulations to investigate the interactions of an electromagnetic field with the nanostructures. A simplified unit model, shown in the inset of Figure 4c, was constructed to calculate the distribution of the local electromagnetic field near the Au−silicon nanostructures. According to the observation of the as-fabricated nanostructures, the period is adopted as 500 nm and the line width is 100 nm. The depth of the nanostructures and the Au layer thickness are expressed as h and t, respectively. The maximal mesh size of the unit cell is set as 3 nm in

DOI: 10.1021/acsami.7b08807
ACS Appl. Mater. Interfaces 2017, 9, 32369−32376

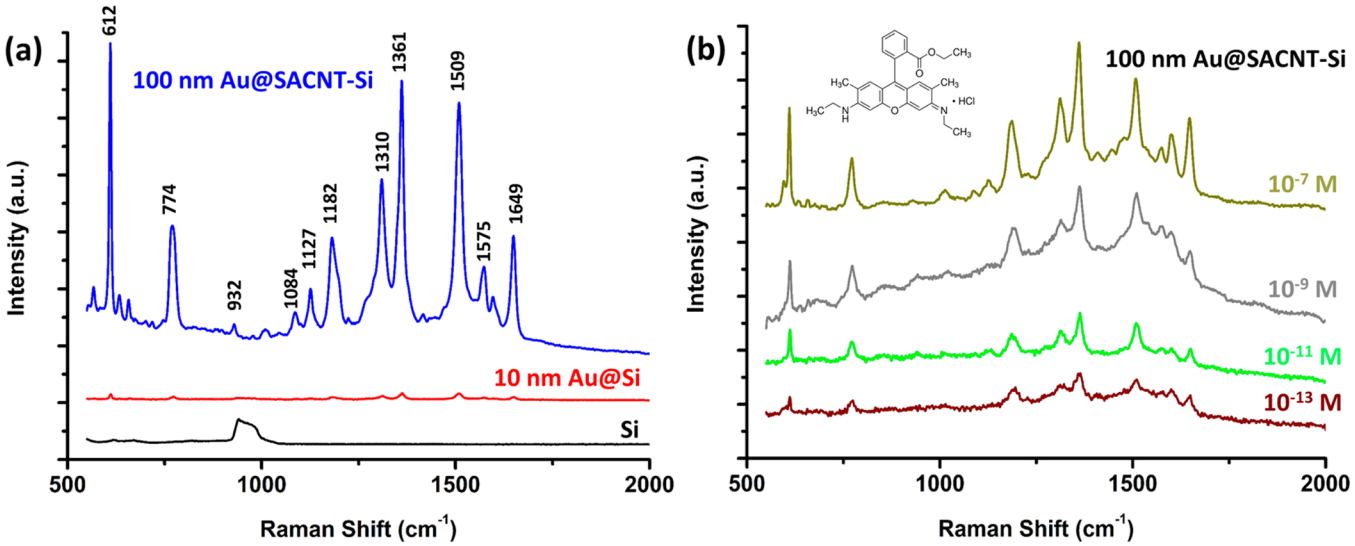

Figure 5. (a) Raman spectra of R6G with concentration of 10^{-6} M on SERS substrate, Au−silicon substrate, and silicon. (b) Raman spectra of SERS substrate, and R6G molecule concentrations from 10^{-7} to 10^{-13} M (from top to bottom). Laser wavelength 632.8 nm, excitation intensity 0.1 mW, data acquisition time 10 s.

simulations, which is fine enough to accurately discretize the nanostructures. In Figure 4b, the SEM image shows local details of the substrate and features of the nanostructures. This image further confirmed the presence of lines with widths of tens of nanometers arranged in the perpendicular direction, which is consistent with the morphology of the SACNT networks. The silicon nanostructures were completely covered by a uniform Au layer, forming the Au−silicon nanostructures.

DISCUSSION

First, we rigorously evaluated the relationship between the Au layer thickness and electromagnetic field intensity at a fixed silicon nanostructure depth of h = 300 nm. The Au−silicon nanostructures were intended to be perpendicularly irradiated by a polarized plane wave with a wavelength of 633 nm. The dielectric permittivity of bulk Au and silicon was acquired from previously published experimental data.[40,41] Figure 4a shows the simulated results for the normalized local electromagnetic field distribution on a cross nanostructure with various Au layer thicknesses. An extraordinarily large electromagnetic field enhancement depicted by a factor of $\left(\frac{E}{E_0}\right)^2$ can be observed, where E represents the amplitude of the maximal local electromagnetic field on the nanostructures and E_0 is that for the incident electromagnetic field. With increasing Au layer thickness, the electromagnetic field enhancement factor increases from 60 to the maximum of 1118, corresponding to Au layer thickness of 100 nm. Thus, the local electromagnetic field of the as-fabricated nanostructure enhanced most significantly with Au thickness of 100 nm.

Simulation was also carried out to study the effect of the nanostructure depth on the intensity of the electromagnetic field, with the thickness of the Au layer fixed at 100 nm, the period of the nanostructures also set at 500 nm, and the line width at 100 nm. As indicated in Figure 4c, with increasing nanostructure depth, the intensity of the electromagnetic field distribution also increased, reaching a maximum at a depth of 300 nm. Then, the enhancement remains almost steady with further increases in the nanostructure depth. With consideration of process feasibility and nanostructure uniformity, the silicon nanostructure depth is set at 500 nm for the SERS substrate. With the Au layer thickness of 100 nm and silicon nanostructure depth of 500 nm optimized, the electromagnetic field distribution of the Au−silicon nanostructures was enhanced most significantly, as depicted in Figure 4d. The structure with such a simple model can also obtain a large electromagnetic field enhancement, indicating that the as-fabricated quasi-periodic network nanostructures can be used as a SERS substrate. Figure S3 also gives Raman enhancement results for the SERS substrate with various parameters, showing that SERS substrates with the aforementioned parameters present the best SERS performance.

To further demonstrate both the sensitivity and reproducibility of the fabrication approach, Raman spectra were also acquired systematically from the SERS substrate using R6G as a probe molecule; both a 10 nm Au-coated bare silicon substrate and bare silicon substrate were employed for comparison. A 10^{-6} M aqueous solution of R6G (Sigma-Aldrich) in deionized water was prepared, and a drop of 20 μL was applied to the SERS substrate. The samples were excited with a 632.8 nm laser with 0.1 mW power through a 100× objective lens (NA 0.9), and the laser spot was 8 μm^2. Because of the fluorescence effects, the laser of 785 nm is always used in the detection of phosmet.[31,32] While in the detection of R6G, fluorescence effects do not appear apparently; thus, 633 nm is commonly used. The resonant condition should be adjusted for various wavelengths for maximized electromagnetic field enhancement. In this manuscript, the calculation and optimization was carried according to the wavelength 632.8 nm. It is a great advantage for these SERS substrates that the resonant condition could be easily optimized and carried on the substrate with different Au layer thicknesses and nanostructure depths according to the excitation wavelength.

As shown in Figure 5a, Raman peaks were greatly enhanced on the as-fabricated SERS substrates and all of the Raman peaks match well with the characteristics of the Raman spectrum of R6G. Generally speaking, because of the limitation of the e-beam deposition process for metal materials, the surface of the as-fabricated metal materials at the scale of a few nanometers was fairly rough and appeared grainy at the micro scale. Thus,

DOI: 10.1021/acsami.7b08807
ACS Appl. Mater. Interfaces 2017, 9, 32369−32376

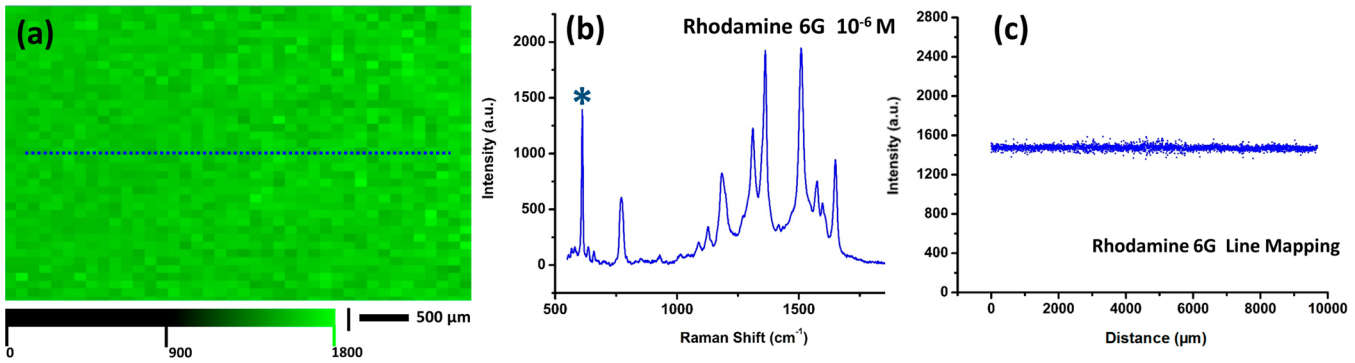

Figure 6. (a) Raman map of 5 × 5 mm area with a laser spot of 8 μm^2 and a step size of 100 μm. The normalized intensity for the 612 cm^{-1} peak across the SERS substrate is shown on a color scale. (b) One typical spectrum of Raman map with 612 cm^{-1} peak labeled. (c) Intensity of the 612 cm^{-1} peak along a 5 mm line on the SERS substrate, with 5% deviation from the average signal.

the Raman signals of R6G molecules were enhanced on the 10 nm Au layer compared with bare silicon. However, the as-fabricated SERS substrates provide plenty more "hot spots" with purposeful design compared with planar metal-deposited silicon substrates. Thus, the results indicate that the Raman signals can be more significantly enhanced on the as-fabricated SERS substrates. For the SERS substrates, one key remaining challenge is to increase the density of the "hot spots" and accessibility to improve the sensitivity of analysis, especially in the realization of matter detection at the single-molecule scale. Thus, Raman spectra of R6G solutions with molecule concentrations ranging from 10^{-7} to 10^{-13} M were acquired to investigate the sensitivity of the as-fabricated SERS substrates. As shown in Figure 5b, the Raman spectra could still be identified with molecule concentrations down to 10^{-13} M. All of the Raman bands match well with the characteristics of the Raman spectrum of R6G, and the corresponding peaks are clearly identified. More importantly, the detection limits of the as-fabricated SERS substrates can reach picomolar or even lower levels, which is comparable to the best results previously published.[4,9,26]

Furthermore, the enhancement factor (EF) of SERS substrates was calculated for evaluation. The results were estimated with the spectra from a 10^{-6} M R6G solution and R6G powder as reference. The enhancement factor was calculated as

$$\mathrm{EF} = \frac{I_{\mathrm{SERS}}}{I_{\mathrm{vol}}} \times \frac{N_{\mathrm{vol}}}{N_{\mathrm{SERS}}} \quad (1)$$

where I_{SERS} is the spectral intensity of R6G on the as-fabricated SERS substrate, N_{SERS} is the estimated number of R6G molecules probed on the SERS substrate I_{vol} is the Raman spectral intensity of a bulk sample, and N_{vol} is the number of R6G molecules probed. The Raman peak at 1509 cm^{-1} was chosen for calculation, and the enhancement factor was calculated to be 1.77×10^8 for the as-fabricated SERS substrate. With comprehensive consideration of the simulation results, it is demonstrated that the Au−silicon nanostructures and related fabrication approach are suitable for SERS applications. As the fabrication process is relatively simple and can be realized over a large area in a cost-effective manner, the SERS substrates are promising for routine use in actual applications (details of the calculation are introduced in Supporting Information S5).

To study the uniformity of Raman signals across a large area, mapping measurements were performed on a substrate with a size of 5 × 5 mm. R6G solution with a concentration of 10^{-6} M was prepared on the SERS substrates, and spectra were recorded every 100 μm across the substrates. In Figure 6a, the intensity of the peak at 612 cm^{-1} is shown as a function of position over the entire substrate. The resulting Raman map is composed of 2500 spectra and shows the relative intensity variation of the peak at 612 cm^{-1}, where one of the spectra is shown in Figure 6b. Over the sample area of 25 mm^2, which is the typical size of current commercial SERS products, the SERS performance of the as-fabricated SERS substrate remained highly uniform. Furthermore, a line scan of the substrate was taken, as denoted by the blue line in Figure 6a. As shown in Figure 6c, the line scan results of the intensity peak at 612 cm^{-1} with a step size of 2 μm exhibit excellent uniformity, with a deviation of less than 5% from the average signal.

As the SACNT films have already been produced automatically over large areas, we endeavored to realize fabrication of the as-fabricated SERS substrate at the wafer scale and make it useful as a routine analytical tool at low cost. As the SERS substrate could be produced at large scale in a cost-effective manner, it is expected that this method will facilitate widespread applications of SERS detection techniques, especially in situations where chemical detection of trace amounts is necessary. Therefore, comparison tests were also performed between commercial SERS products and the samples fabricated in this study. With the probe molecule 1,2-bis(4-pyridyl)ethylene (BPE) at low concentration, which is commonly used as a standard sample in commercial SERS tests, the as-fabricated SERS substrate also exhibits excellent signal enhancement (as shown in the Supporting Information, Figure S6). With two commercially available substrates used as a benchmark under identical conditions, the SERS substrate in this study shows competitive performance.

CONCLUSION

In conclusion, this study presents a cost-effective fabrication approach for SERS substrates with a uniform silicon nanostructure over a large area. Significantly, with the advantage of nanoscale features and the high density of the as-fabricated nanostructure, high-density SERS hot spots are generated and the SERS substrate shows a high enhancement factor and excellent reproducibility. Detection of trace amounts of various materials has been realized on the SERS substrates, with the lowest concentration down to picomolar level. In particular, the SERS substrate can be applied in pesticide residue detection of phosmet with a detection limit as low as

DOI: 10.1021/acsami.7b08807
ACS Appl. Mater. Interfaces 2017, 9, 32369−32376

10^{-9} M (0.03 ppb), which is 2 orders of magnitude lower than the maximal residue limit allowed for food safety. The as-fabricated SERS substrates have been already realized at 4 in. wafer scale and prepared as consumables for actual use, showing remarkable uniformity with a deviation of less than 5%. Furthermore, it is strongly believed that this simple and cost-effective approach will facilitate widespread use of SERS sensing for trace amounts.

■ ASSOCIATED CONTENT

Supporting Information

The Supporting Information is available free of charge on the ACS Publications website at DOI: 10.1021/acsami.7b08807.

Images of the fabrication process of SACNT films, introduction of the ICP process for silicon nanostructures in detail, simulation results for nanostructure parameter optimization and corresponding Raman spectra results, calculation of enhancement factors for SERS substrates, and Raman spectra comparison for SERS substrates and commercial products (PDF)

■ AUTHOR INFORMATION

Corresponding Author

*Tel.: +86 10 62796019. Fax: +86 10 62792457. E-mail: QunqLi@mail.tsinghua.edu.cn.

ORCID

Qunqing Li: 0000-0001-9565-0855

Author Contributions

#These authors contributed equally.

Notes

The authors declare no competing financial interest.

■ ACKNOWLEDGMENTS

This work was financially supported by the National Natural Science Foundation of China (11574171, 90921012) and China Postdoctoral Science Foundation (2016M601012).

■ REFERENCES

(1) Fleischmann, M.; Hendra, P. J.; Mcquillan, A. J. Raman Spectra of Pyridzne adsorbed at a Silver Electrode. *Chem. Phys. Lett.* **1974**, *26*, 163−166.

(2) Mcquillan, A. J.; Hendra, P. J.; Fleischmann, M. Raman Spectroscopic Investigation of Silver Electrode. *J. Electroanal. Chem. Interfacial Electrochem.* **1975**, *65*, 933−944.

(3) Tzolov, M. B.; Tzenov, N. V.; Dimova Malinovska, D. I.; Yankov, D. Y. Surface-Enhanced Raman Scattering of Amorphous Silicon-Carbon Films. *Appl. Phys. Lett.* **1993**, *62*, 2396−2398.

(4) Lin, S.; Zhu, W.; Jin, Y.; Crozier, K. B. Surface-Enhanced Raman Scattering with Ag Nanoparticles Optically Trapped by a Photonic Crystal Cavity. *Nano Lett.* **2013**, *13*, 559−563.

(5) Lin, D.; Wu, Z.; Li, S.; Zhao, W.; Ma, C.; Wang, J.; Jiang, Z.; Zhong, Z.; Zheng, Y.; Yang, X. Large-Area Au-Nanoparticle-Functionalized Si Nanorod Arrays for Spatially Uniform Surface-Enhanced Raman Spectroscopy. *ACS Nano* **2017**, *11*, 1478−1487.

(6) Hoang, P.; Khashab, N. M. Non-Resonant Large Format Surface Enhanced Raman Scattering Substrates for Selective Detection and Quantification of Xylene Isomers. *Chem. Mater.* **2017**, *29*, 1994−1998.

(7) Yigit, M. V.; Zhu, L.; Ifediba, M. A.; Zhang, Y.; Carr, K.; Moore, A.; Medarova, Z. Noninvasive MRI-SERS Imaging in Living Mice Using an Innately Bimodal Nanomaterial. *ACS Nano* **2011**, *5*, 1056−1066.

(8) Ando, J.; Fujita, K.; Smith, N. I.; Kawata, S. Dynamic SERS Imaging of Cellular Transport Pathways with Endocytosed Gold Nanoparticles. *Nano Lett.* **2011**, *11*, 5344−5348.

(9) Kim, S.; Piao, L.; Han, D.; Kim, B. J.; Chung, T. D. Surface Enhanced Raman Scattering on Non-SERS Active Substrates and In Situ Electrochemical Study based on a Single Gold Microshell. *Adv. Mater.* **2013**, *25*, 2056−2061.

(10) Tan, Y.; Gu, J.; Xu, L.; Zang, X.; Liu, D.; Zhang, W.; Liu, Q.; Zhu, S.; Su, H.; Feng, C.; Fan, G.; Zhang, D. High-Density Hotspots Engineered by Naturally Piled-Up Subwavelength Structures in Three-Dimensional Copper Butterfly Wing Scales for Surface-Enhanced Raman Scattering Detection. *Adv. Funct. Mater.* **2012**, *22*, 1578−1585.

(11) Tang, S.; Li, Y.; Huang, H.; Li, P.; Guo, Z.; Luo, Q.; Wang, Z.; Chu, P. K.; Li, J.; Yu, X. Efficient Enrichment and Self-Assembly of Hybrid Nanoparticles into Removable and Magnetic SERS Substrates for Sensitive Detection of Environmental Pollutants. *ACS Appl. Mater. Interfaces* **2017**, *9*, 7472−7480.

(12) Lim, D.; Jeon, K.; Hwang, J.; Kim, H.; Kwon, S.; Suh, Y. D.; Nam, J. Highly Uniform and Reproducible Surface-Enhanced Raman Scattering from DNA-tailorable Nanoparticles with 1-nm Interior Gap. *Nat. Nanotechnol.* **2011**, *6*, 452−460.

(13) Lang, X.; Qiu, T.; Yin, Y.; Kong, F.; Si, L.; Hao, Q.; Chu, P. K. Silver Nanovoid Arrays for Surface-Enhanced Raman Scattering. *Langmuir* **2012**, *28*, 8799−8803.

(14) Liu, K.; Bai, Y.; Zhang, L.; Yang, Z.; Fan, Q.; Zheng, H.; Yin, Y.; Gao, C. Porous Au−Ag Nanospheres with High-Density and Highly Accessible Hotspots for SERS Analysis. *Nano Lett.* **2016**, *16*, 3675−3681.

(15) Rodríguez-Lorenzo, L.; Álvarez-Puebla, R. A.; de Abajo, F. J. G.; Liz-Marzán, L. M. Surface Enhanced Raman Scattering Using Star-Shaped Gold Colloidal Nanoparticles. *J. Phys. Chem. C* **2010**, *114*, 7336−7340.

(16) Li, P.; Li, Y.; Zhou, Z.; Tang, S.; Yu, X.; Xiao, S.; Wu, Z.; Xiao, Q.; Zhao, Y.; Wang, H.; Chu, P. K. Evaporative Self-Assembly of Gold Nanorods into Macroscopic 3D Plasmonic Superlattice Arrays. *Adv. Mater.* **2016**, *28*, 2511−2517.

(17) Baker, G. A.; Moore, D. S. Progress in Plasmonic Engineering of Surface-enhanced Raman-scattering Substrates toward Ultra-trace Analysis. *Anal. Bioanal. Chem.* **2005**, *382*, 1751−1770.

(18) Banholzer, M. J.; Millstone, J. E.; Qin, L.; Mirkin, C. A. Rationally Designed Nanostructures for Surface-enhanced Raman Spectroscopy. *Chem. Soc. Rev.* **2008**, *37*, 885.

(19) Yang, D.; Cho, H.; Koo, S.; Vaidyanathan, S. R.; Woo, K.; Yoon, Y.; Choo, H. Simple, Large-Scale Fabrication of Uniform Raman-Enhancing Substrate with Enhancement Saturation. *ACS Appl. Mater. Interfaces* **2017**, *9*, 19092−19101.

(20) Oh, Y.; Jeong, K. Glass Nanopillar Arrays with Nanogap-Rich Silver Nanoislands for Highly Intense Surface Enhanced Raman Scattering. *Adv. Mater.* **2012**, *24*, 2234−2237.

(21) Schmidt, M. S.; Hübner, J.; Boisen, A. Large Area Fabrication of Leaning Silicon Nanopillars for Surface Enhanced Raman Spectroscopy. *Adv. Mater.* **2012**, *24*, 11−18.

(22) Zhou, Q.; Zhang, X.; Huang, Y.; Li, Z.; Zhao, Y.; Zhang, Z. Enhanced Surface-enhanced Raman Scattering Performance by Folding Silver Nanorods. *Appl. Phys. Lett.* **2012**, *100*, 113101.

(23) Zhang, B.; Wang, H.; Lu, L.; Ai, K.; Zhang, G.; Cheng, X. Large-Area Silver-Coated Silicon Nanowire Arrays for Molecular Sensing Using Surface-Enhanced Raman Spectroscopy. *Adv. Funct. Mater.* **2008**, *18*, 2348−2355.

(24) Lee, S. Y.; Hung, L.; Lang, G. S.; Cornett, J. E.; Mayergoyz, I. D.; Rabin, O. Dispersion in the SERS Enhancement with Silver Nanocube Dimers. *ACS Nano* **2010**, *4*, 5763−5772.

(25) Cho, W. J.; Kim, Y.; Kim, J. K. Ultrahigh-Density Array of Silver Nanoclusters for SERS Substrate with High Sensitivity and Excellent Reproducibility. *ACS Nano* **2012**, *6*, 249−255.

(26) Kumar, C. S. S. R. *Raman Spectroscopy for Nanomaterials Characterization*; Springer: Berlin, 2012.

(27) Liu, Z.; Yang, Z.; Peng, B.; Cao, C.; Zhang, C.; You, H.; Xiong, Q.; Li, Z.; Fang, J. Highly Sensitive, Uniform, and Reproducible

Surface-Enhanced Raman Spectroscopy from Hollow Au-Ag Alloy Nanourchins. *Adv. Mater.* **2014**, *26*, 2431−2439.
(28) Balasubramanian, K.; Zuccaro, L.; Kern, K. Tunable Enhancement of Raman Scattering in Graphene-Nanoparticle Hybrids. *Adv. Funct. Mater.* **2014**, *24*, 6348−6358.
(29) Zhu, Z.; Li, Q.; Bai, B.; Fan, S. Reusable Three-dimensional Nanostructured Substrates for Surface-enhanced Raman Scattering. *Nanoscale Res. Lett.* **2014**, *9*, 25−32.
(30) Kanipe, K. N.; Chidester, P. P. F.; Stucky, G. D.; Moskovits, M. Large Format Surface-Enhanced Raman Spectroscopy Substrate Optimized for Enhancement and Uniformity. *ACS Nano* **2016**, *10*, 7566−7571.
(31) Jiang, K.; Wang, J.; Li, Q.; Liu, L.; Liu, C.; Fan, S. Superaligned Carbon Nanotube Arrays, Films, and Yarns: A Road to Applications. *Adv. Mater.* **2011**, *23*, 1154−1161.
(32) Wei, Y.; Lin, X.; Jiang, K.; Liu, P.; Li, Q.; Fan, S. Thermoacoustic Chips with Carbon Nanotube Thin Yarn Arrays. *Nano Lett.* **2013**, *13*, 4795−4801.
(33) Feng, C.; Liu, K.; Wu, J.; Liu, L.; Cheng, J.; Zhang, Y.; Sun, Y.; Li, Q.; Fan, S.; Jiang, K. Flexible, Stretchable, Transparent Conducting Films Made from Superaligned Carbon Nanotubes. *Adv. Funct. Mater.* **2010**, *20*, 885−891.
(34) Jin, Y.; Li, Q.; Chen, M.; Li, G.; Zhao, Y.; Xiao, X.; Wang, J.; Jiang, K.; Fan, S. Large area Nanoscale Metal Meshes for Use as Transparent Conductive Layers. *Nanoscale* **2015**, *7*, 16508−16515.
(35) Jin, Y.; Li, Q.; Chen, M.; Li, G.; Zhao, Y.; Xiao, X.; Wang, J.; Jiang, K.; Fan, S. Study of Carbon Nanotubes as Etching Masks and Related Applications in the Surface Modification of GaAs-based Light-Emitting Diodes. *Small* **2015**, *11*, 4111−4116.
(36) Zhang, L.; Jiang, C.; Zhang, Z. Graphene Oxide Embedded Sandwich Nanostructures for Enhanced Raman Readout and their Applications in Pesticide Monitoring. *Nanoscale* **2013**, *5*, 3773.
(37) Dhakal, S.; Li, Y.; Peng, Y.; Chao, K.; Qin, J.; Guo, L. Prototype Instrument Development for Non-destructive Detection of Pesticide Residue in Apple Surface using Raman technology. *J. Food Eng.* **2014**, *123*, 94−103.
(38) Liu, B.; Han, G.; Zhang, Z.; Liu, R.; Jiang, C.; Wang, S.; Han, M. Shell Thickness-Dependent Raman Enhancement for Rapid Identification and Detection of Pesticide Residues at Fruit Peels. *Anal. Chem.* **2012**, *84*, 255−261.
(39) Fan, Y.; Lai, K.; Rasco, B. A.; Huang, Y. Analyses of Phosmet Residues in Apples with Surface-enhanced Raman Spectroscopy. *Food Control* **2014**, *37*, 153−157.
(40) Johnson, P. B.; Christy, R. W. Optical Constants of the Noble Metals. *Phys. Rev. B* **1972**, *6*, 4370−4379.
(41) Palik, E. D. *Handbook of Optical Constants of Solids*; Academic Press: San Diego, 1985.

DOI: 10.1021/acsami.7b08807
ACS Appl. Mater. Interfaces 2017, 9, 32369−32376